JOINT EUROPEAN TORUS JET

JET–P(93)106

O. Pogutse, W. Kerner, V. Gribkov, S. Bazdenkov, M. Osipenko

The Resistive Interchange Convection in the Edge of Tokamak Plasmas

The Resistive Interchange Convection in the Edge of Tokamak Plasmas

O. Pogutse, W. Kerner, V. Gribkov[1], S. Bazdenkov[1], M. Osipenko[1]

JET-Joint Undertaking, Culham Science Centre, OX14 3DB, Abingdon, UK

[1]Russian Scientific Centre, Kurchatov Institute, Moscow, Russia.

Preprint of a paper to be Submitted for publication in
Plasma Physics and Controlled Fusion
January 1994

ABSTRACT

This paper is devoted to a summary of previous and new theoretical results concerning the behaviour of plasmas outside the separatrix i.e. in the region where the magnetic field lines do not form closed magnetic surfaces.

The resistive interchange model is used to describe selfconsistently the generation of poloidal (or toroidal) flow and the onset of ELMs, which appear as bubbles of increased density (or higher temperature). In addition, the decrease of the turbulent transport processes as the velocity of the flow increases and its connection with the L-H transition are discussed. The linear theory of stability is applied and complemented by a full numerical simulation of the two-dimensional nonlinear equations. Analytic solutions for asymptotically small parameters in the nonlinear model are derived and used for the explanation of the numerical results. Semi-phenomological turbulence balance equations for the resistive interchange convection are presented as well. Finally, these results are applied for the explanation of existing experiments.

1. INTRODUCTION

In recent tokamak experiments specific MHD activity was observed at the plasma periphery [1]-[3]. More detailed investigations have shown that these oscillations (so-called edge localised modes ELMs) sometimes look like dumping of density and temperature filaments into the scrape-off layer, which leads to the quasi-periodical oscillations of the particle and energy fluxes. ELMs are observed during H-mode discharges in JET [4] with widely varying amplitudes and repetition rates. Some of the ELMs are similar to the ELMs in DIII-D [5] and ASDEX [3]. Data from ASDEX show, that the edge turbulence is essentially two-dimensional and perpendicular to the magnetic field. Flute-like instabilities lead to the convection of flux-bundles at the edge [1]. In similar cases the TFTR data [2] demonstrate the dumping of electrons, namely radially localised electron temperature perturbations appear at the plasma edge and move radially outwards. Prior to these singular ELMs in JET, the pressure gradients near the edge plasma are found to be well below the ideal ballooning stability limit, while resistive ballooning modes can become unstable.

To elucidate the nature of the ELMs the following model was proposed in our previous papers [6]: The dissipative flute-like resistive interchange instability at

the plasma edge is considered, where the parallel dissipation along the magnetic field lines is taken into account for the flux-tube with the ends at the divertor plates or at the limiter. In contrast to the resistive instability inside the separatrix, which has the character of a three-dimensional resistive ballooning mode, the instability in the SOL is basically two-dimensional. This strongly simplifies its examination. This is mainly a mathematical aspect. From the physical point of view the lack of closed magnetic surfaces near the plasma edge permits the manifestation of instabilities which are forbidden in the bulk plasma. In this case the flute-like instability in the SOL region of tokamaks has the characteristic feature of flute-like instabilities in open systems. The first major point is that the effect of the magnetic field line curvature is not averaged over a flux surface, which implies that the contribution to the instability is of first order in the inverse aspect ratio $\varepsilon = r/R$ (r and R are the minor and major tokamak radii. This makes it different from the ε^2 effect appearing in the usual ballooning mode model. This clearly is a destabilizing effect. The inclusion of longitudinal conductivity leads to a stabilising effect and the final result is determined by the competition of these two tendencies defining the characteristic perpendicular dimension of the perturbations. This plays an important role in the discussion. The second major point is that due to the open end region the perturbations can be chosen with good accuracy in two-dimensional form.

The outline of this work is as follows. In Section 2 the general equations for resistive interchange are introduced; in Section 3 the linear theory of these equations is discussed; in Section 4 results of the two-dimensional numerical simulation are analysed. In Section 5 the properties of two simplified phenomenological and more elaborated low-mode number systems are discussed, which help us to reproduce qualitatively the main nonlinear results and which form the basis for our model of the anomalous transport. In Section 6 the results of the resistive interchange theory are compared with the experiments.

2. PHYSICAL MODEL

As a typical example of a tokamak with a separatrix we chose an ASDEX-like geometry (Fig. 1). In the limit of a strong magnetic field, the system is described by the following equations:

The vortex equation:

$$\frac{cMn_0}{B^2}\,\frac{d\Delta_\perp\phi}{dt} + \left[\nabla P \times \nabla \frac{1}{B}\right]_z = \frac{1}{c}\left(\vec{b}\cdot\nabla\right)j_z + \frac{cMn_0}{B^2}\mu_\perp\,\Delta_\perp^2\phi. \qquad (1)$$

Here $\frac{d}{dt} = \frac{\partial}{\partial t} + \underline{v}_\perp \cdot \nabla$, where $\underline{v}_\perp$ is expressed as

$$\underline{v}_\perp = \frac{c}{B}\left[\underline{e}_z \times \nabla\phi\right] \qquad (2)$$

P is the total pressure $P = P_e + P_i$. M denotes the mass of the ions, c the velocity of light and $\mu_\perp$ the transverse viscosity coefficient; n is the density.

The magnetic field is expressed by a vector potential with the following notations:

$$\vec{B} = B*\vec{b} = B_z*\vec{e}_z - \left[e_z \times \nabla A_z\right],\ B_z = B_0*(1 - x/R),\ x = R - R_0, \qquad (3)$$

with

$$j_z = -\,c/4\pi*\Delta_\perp A_z. \qquad (4)$$

Then the parallel component of the electron equation of motion yields:

$$\frac{\partial A_z}{\partial t} + c\left(\vec{b}\cdot\nabla\right)\phi = -\,c\frac{j_z}{\sigma} + \frac{c}{en_0}\left(\vec{b}\cdot\nabla\right)P_e, \qquad (5)$$

with σ the conductivity.

The continuity equation reads:

$$\frac{\partial n}{\partial t} + (v_\perp\cdot\nabla)n = \frac{1}{e}\left(\vec{b}\cdot\nabla\right)j_z + D_\parallel\Delta_\parallel n + D_\perp\Delta_\perp n. \qquad (6)$$

$D_\parallel$, $D_\perp$ are the longitudinal and transverse diffusion coefficients.

Instead of the energy equation we use the condition T_e = const. We also have investigated the case when the energy equation has been used and the condition n = const has been applied leading to qualitatively the same results.

For the resistive interchange instability we get in the electrostatic limit:

$$j_z = -\sigma * \nabla_{\parallel} \left(\phi - \frac{T_e}{n_0} \tilde{n} \right). \tag{7}$$

Thus, we can use two equations in this case instead of three. In dimensionless form, these read:

$$\frac{\partial \Delta_{\perp} \phi}{\partial t} + \left[\nabla \phi \times \nabla \Delta \phi \right]_z + g_B * \frac{\partial \tilde{n}}{\partial y} + \sigma_1 * \nabla_{\parallel}^2 \left[\phi - \xi * \tilde{n} \right] = \Delta_{\perp} \mu_{\perp} \Delta_{\perp} \phi, \tag{8}$$

$$\frac{\partial \tilde{n}}{\partial t} + \left[\nabla \phi \times \nabla \tilde{n} \right]_z + g_n * \frac{\partial \phi}{\partial y} + \sigma_2 * \nabla_{\parallel}^2 \left[\phi - \xi * \tilde{n} \right] = D_{\parallel} \nabla_{\parallel}^2 \tilde{n} + \nabla_{\perp} D_{\perp} \nabla_{\perp} \tilde{n}. \tag{9}$$

Here the density is decomposed into its initial value and fluctuating nonlinear component, i.e.

$$n = n_0 + \tilde{n}.$$

After averaging along the field lines, these equations take the following form:

$$\frac{\partial \Delta_{\perp} \phi}{\partial t} + \left[\nabla \phi \times \nabla \Delta \phi \right]_z + g_B \frac{\partial \tilde{n}}{\partial y} + \sigma_1 * \left[\phi - \bar{\phi} - \xi * \left(\tilde{n} - \bar{n} \right) \right] = \Delta_{\perp} \mu_{\perp} \Delta_{\perp} \phi, \tag{10}$$

$$\begin{aligned} &\frac{\partial \tilde{n}}{\partial t} + \left[\nabla \phi \times \nabla \tilde{n} \right]_z + g_n \frac{\partial \phi}{\partial y} = \sigma_2 * \left[\phi - \bar{\phi} - \xi * \left(\tilde{n} - \bar{n} \right) \right] + \\ &1 / \tau_{\parallel} * \left(\tilde{n} - \bar{n} \right) + \nabla_{\perp} D_{\perp} \nabla_{\perp} \tilde{n}. \end{aligned} \tag{11}$$

Since the operator $\nabla_{\parallel}$ does only act on the part of the perturbation which depends on y, the average values of ϕ and n, where $\bar{a}(x) = \oint a(x,y)\, dy$, need to be subtracted in Eqs. (10) and (11).

Here we introduce the following dimensionless parameters:

$g_n \equiv g_n(x) = -\frac{x_0 *}{n_0} \frac{\partial n_0(x)}{\partial x}$ is a function of order unity, n_0 the characteristic density, x_0 the characteristic scale length for the density, for example: the linear profile: $n_0(x) = n_0 * (1 - x / x_0)$ has $g_n = 1$. $g_B = \frac{R_o}{R}$ where R_o is a typical length.

If we chose the characteristic time $t_0 = (x_0 * R_0) / C_s$ as the typical time for the interchange instability then with $\rho_s = (T_e / M)^{1/2} / \omega_{Bi}$; we have

$$\xi = \rho_s * R_0^{1/2} / x_0^{3/2};$$

$$\sigma_1 = (\tau_s / \tau_A) * \beta^{-1/2} * \left(x_0^3 * R_o\right)^{1/2} / L_\parallel^2;$$

$$\sigma_2 = (\tau_s / \tau_A) * c * x_0 / \left(\omega_{pi} L_\parallel^2\right) = \sigma_1 * \rho_s / (x_0 R_o)^{1/2};$$

$$\tau_s = 4\pi \sigma x_0^2 / c^2;$$

$$\tau_A = x_0 / c_A; \quad \phi = B * x_0^2 / (c * t_0) * \phi; \quad \tilde{n} = \tilde{n} / n_0;$$

$$\tau_\parallel = L_\parallel^2 / (D_\parallel * t_0); \quad \mu_\perp = \mu_\perp * t_0 / x_0^2; \quad D_\perp = D_\perp * t_0 / x_0^2.$$

The order of magnitude of the dimensionless parameters is best demonstrated for typical ASDEX parameters:

$B = 3T$, $T = 100eV$, $R = 1m$, $n_0 = 10^{13} cm^{-3}$, $x_0 = 0.01m$, $Z_{eff} = 3$,

$L_\parallel = c_1 * \pi * q * R_o$, where $c_1 \approx 1$. For these values:

$t_0 \approx 10^{-6} s$, $\rho_s \approx 3 * 10^{-2} cm$,

$\xi \approx 0.3$,

$\tau_s \approx 5 * 10^{-5} s$, $\tau_A \approx 10^{-9} s$,

$\sigma_1 \approx 8 / c_1^2$,

$\sigma_2 \approx 2.4 * 10^{-2} / c1^2 << \sigma_1$,

$D_0 = x_0^2 / t_0 \approx 10^6 cm^2 / s$,

$\tau_\parallel \approx c_1 * 10^{-4} s$.

Here c_1 is the coefficient in the relation $L_{\|} = c_1 * \pi * q * R_o$. It can be somewhat larger by a factor 2 to 3 depending on the separatrix geometry. For the case of the toroidal diaphragm $c_1 = 1$.

The most important parameters in these equations are σ_1 and ξ. If $\xi \approx 1$ then the drift waves play the important role and the resistive interchange instabilities are less important. The coefficient σ_1 introduces the intrinsic spatial scale length (see next Section 3), and strongly influences the turbulent transport.

3. LINEAR THEORY AND DIMENSIONAL ESTIMATES

For linear perturbations the well known dispersion relation follows from the initial equations (1) - (6):

$$\left[\gamma + k_{\perp}^2 * \mu_{\perp}\right] - \frac{\omega_g^2 * \left(k_y^2 / k_{\perp}^2\right)}{\left[\gamma + 1/\tau_{\|} + k_{\perp}^2 * D_{\perp}\right]} + \frac{k_{\|}^2 * C_A^2}{\left[\gamma + k_{\perp}^2 * D_M\right]} = 0 \qquad (12)$$

where $\omega_g^2 = \frac{T_0}{RM} * \frac{dn_0}{n_0 dx} \equiv \frac{C_s^2}{x_0 R}$, $\frac{1}{x_0} = -\frac{dn_0}{n_0 dx}$, $C_A^2 = \frac{B_0^2}{4\pi M n_0}$, $D_M = \frac{c^2}{4\pi\sigma}$.

Let us review the main properties of this equation. For the dissipativeless case it assumes the form:

$$\gamma^2 = \omega_g^2 * \frac{k_y^2}{k_{\perp}^2} - k_{\|}^2 * C_A^2, \qquad (13)$$

i.e. it describes the mixture of flute and Alfven modes. The last term gives a stabilisation due to the end conditions. If we estimate $k_{\|}$ as $1/L_{\|}$, where $L_{\|}$ is the length of the interchange localisation, then the condition of stability for the ideal case can be written as: $C_s^2/(x_0 R) < C_A^2 / L_{\|}^2$. For $L_{\|} \sim \pi * q * R$ this can be expressed as follows:

$$\beta < \varepsilon / (\pi * q)^2. \qquad (14)$$

This condition is usually fulfilled at the boundary of the plasma.

If we now take into account the dissipation, slower dissipative instabilities can occur despite Eq. (14). These instabilities exist if

$$\gamma << k_\perp^2 * D_M. \tag{15}$$

It immediately follows that $D_{RI} < D_M$ where $D_{RI} = \gamma / k_\perp^2$ denotes the diffusion coefficient of the resistive interchange and $D_M = c^2/(4\pi\sigma)$, the so-called pseudoclassical coefficient of diffusion.

In this electrostatic limit the dispersion, Eq. (12), relation has the form:

$$\left[\gamma + k_\perp^2 * \mu_\perp + \frac{k_\parallel^2 * C_A^2}{k_\perp^2 * D_M}\right] * \left[\gamma + 1/\tau_\parallel + k_\perp^2 * D_\perp\right] = \omega_g^2 * \frac{k_y^2}{k_\perp^2}. \tag{16}$$

The main dissipative term here is $\frac{k_\parallel^2 * C_A^2}{k_\perp^2 * D_M}$, which describes charge losses at the end plates.

From (16) it follows, that the maximum growth rate is $\gamma_0 \sim \omega_g = 1/t_0$ and the characteristic wave number is

$$k_0^2 = C_A^2 / \left(L_\parallel^2 * D_M * \omega_g\right). \tag{17}$$

Small terms connected with $\mu_\perp$, $D_\perp$, $1/\tau_\parallel$ are negligible for these estimates. The relation (17) separates the pure hydrodynamical model $(k_0 * x_0 < 1)$ from the plasma model $(k_0 * x_0 > 1)$; this boundary also coincides with the condition $\sigma_1 = 1$. In the plasma case we have the following independent parameters:

$$\gamma_0,\ k_0,\ x_0,\ \tau_\parallel,\ \mu_\perp,\ D_\perp. \tag{18}$$

If we suppose that $\mu_\perp \sim D_\perp$ and are defined selfconsistently by the resistive interchange turbulence, then from dimensional considerations we can write:

$$\mu_\perp \sim D_\perp \sim \left(\gamma_0 / k_0^2\right) * F(\gamma_0 * \tau_\parallel,\ k_0 * x_0) \sim \left(\gamma_0 / k_0^2\right) * f(\gamma_0 * \tau_\parallel), \tag{19}$$

where f is some dimensionless function of order unity. The last proportionality in Eq. (19) follows from the assumed weak dependence of the function F on $(k_0 * x_0)$.

This result is correct only for fully developed turbulence, when the viscosity and thermal conductivity are sufficiently small, i.e. $\mu_\perp / \left(\gamma_0 / k_0^2\right) << 1$, $D_\perp / \left(\gamma_0 / k_0^2\right) << 1$. For the experimental conditions and especially for our numerical modeling this asumption is not a very good approximation (for example if $D_\perp / \left(\gamma_0 / k_0^2\right) \sim 0.01$ then we have only in the order of ten harmonics in the spectrum of the potential). Therefore, a general expression for turbulent diffusion should look as follows:

$$\mu_\perp{}^{turb} \sim D_\perp{}^{turb}{}_\perp \sim \left(\gamma_0 / k_0^2\right) * F\left(D_\perp / \left(\gamma_0 / k_0^2\right),\ \gamma_0 * \tau_\parallel,\ k_0 * x_0\right), \qquad (20)$$

where the function F, can be obtained from numerical experiments. Analogous expressions for other quantities can be given, for example, the average velocity V_0 has the form:

$$V_0 \sim \left(\gamma_0 / k_0\right) * F_1\left(D_\perp / \gamma_0 / k_0^2\right),\ \gamma_0 * \tau_\parallel,\ k_0 * x_0), \qquad (21)$$

where F_1 is the other dimensionless function. The numerical simulations yield $F_1 \simeq 1$.

4. NUMERICAL SIMULATION

The system of equations (10)-(11) is solved numerically (for $\sigma_2 = 0$) for rigid wall ($\phi = 0$, $\tilde{n} = 0$) and for free-slip ($\Delta\phi = 0$) boundary conditions at the planes x = 0, x = 1 and with periodicity in the y direction. The numerical scheme is based on two-dimensional finite differences with second order accuracy. Typically, a 32 x 32 grid is used. For the time stepping the second order accurate Lax-Wendroff scheme is applied. The conservation laws are checked and yield a criterion for the accuracy and for the stability of the calculations. The main parameters of this problem are g_B ($g_n = 1$), the transverse viscosity $\mu_\perp$, and diffusivity $D_\perp$ and the longitudinal conductivity σ. As typical output values we take two-dimensional pictures of the convective flow, of the average (over y) poloidal velocity $\overline{V}(x,t)$ and of the density $\overline{n}(x,t)$, the value of the particle flux on the

boundary $q_x(t) = -D_\perp * \frac{\partial \bar{n}}{\partial x}$, and its time average $Q = \lim_{\tau\to\infty} \frac{1}{\tau} * \int_0^\tau q_x(t)dt$. Here the bar denotes the average with respect to y.

The results of the numerical simulations show the strong effect of the sheared flow generation by convective cells due to the Raleigh-Taylor instability. As far as we know this effect has not been observed in the Boussinesq equations previously (our equations (10) - (11) coincide with the Boussinesq equations if σ_1, σ_2 are equal to zero and $\tau_\parallel = \infty$), because the Raleigh-Taylor convection has been usually studied, both experimentally and theoretically, for the bounded model with respect to the y-direction. For the tokamak edge plasma the periodicity constraint in the y-direction and the free-slip rigid planes at x = 0, 1 appear to be more adequate boundary conditions. The effect of the spontaneous generation of the flow is very effective: the value of the flow velocity in dimensionless parameters is of order unity.

When the system is far above the stability threshold $\left(\mu_\perp / \left(\gamma_0 / k_0^2\right) << 1,\ D_\perp / \left(\gamma_0 / k_0^2\right) << 1\right)$, the velocity profile is close to sinoidal form and the shear, V′, experiences quasiperiodical oscillations in time corresponding to the spikes of the density (or heat) flux at the boundary, which can be interpreted as ELMs. Let us now describe the results of the numerical calculations in more detail. If g_B is sufficiently large, $g_B >= 5$, and the typical values of the parameters $\mu_\perp / \left(\gamma_0 / k_0^2\right)$ and $D_\perp / \left(\gamma_0 / k_0^2\right)$ in subsequent calculations are chosen in the order of 0.1, a clear quasiperiodical behaviour of the instability takes place (see Fig. 2). At first the fluctuations of the potential grow and this effect causes the flux on the edge of the plasma to increase. When the fluctuations become sufficiently large an average velocity sets in, it grows up to order unity and then the velocity begins to suppress the fluctuations. After the fluctuations have disappeared the average velocity also disappears and the process repeats itself.

On Fig. 3 the amplitude of the mean velocity and the amplitude of the flux on the boundary are plotted as a function of σ_1. The quantities are averaged over a period of five spikes. For the interval $0 < \sigma_1 < 1$, the dependence is weak. Therefore, it is more interesting to study larger values of σ_1.

The dependence of these quantities on $\mu_\perp$ ($D_\perp = \mu_\perp$) is plotted on Fig. 4. Here the picture displays more detail. The shear velocity decreases monotonously with increasing $\mu_\perp$ and drops approximately by a factor of three with $\mu_\perp$ increasing twenty times. The period between spikes becomes shorter. The flux increases at lower values, assumes a maximum at $\mu_\perp \sim 0.1$ and then suddenly drops. This dependence is explained by the change of the character of the instability. With increasing $\mu_\perp$ the instability changes from quasiperiodical to purely oscillatory behaviour with increasing frequency and then the oscillations dampen out. It should be noted that, when the oscillations of the shear velocity experience damping, the average value of V does not vanish. The particle flux on the boundary becomes constant.

All these results were obtained with a value for $g_B = 10$. In this case the process is quasiperiodical (excluding the case of large $\mu_\perp$ when the oscillations are absent). The numerical simulations of the system (10) - (11) for different g_B allowed us to study the effect of strong suppression of the flux on the boundary which can be considered as a model of the L-H transition. On Fig. 5 the flux q_x is plotted in dependence of g_B for different values of σ_1. For $g_B < 0.05$, which is lower than the threshold of the instability, the flux does not change. With increasing g_B convective flow sets in, the flux q_x is constant in time but increases with g_B. Further increase of g_B leads first to oscillations in q_x and then, for $g_B > 5$, to quasiperiodical spikes (ELMs). With the appearance of oscillations the particle (or heat) flux drops and, as ELMs appear, the flux approaches a constant level. This transition is very sensitive to σ_1. This transition manifests itself for σ_1 values in the narrow interval $0.05 < \sigma_1 < 0.3$, where the flux drops by a factor of 2 - 3. For other values of σ_1 this drop amounts to only 10 - 25%. It should be noted that for the chosen parameters only few harmonics (about ten) grow significantly during the calculations.

5. SIMPLIFIED MODELS FOR THE RESISTIVE INTERCHANGE INSTABILITY

For an explanation of our numerical results and for a prediction of the nonlinear behaviour we discuss two simplified models. The first model is applied to the fully developed turbulent case [6] (which we can not simulate directly) and the second one to the small-parametric case [10] being relevant for our numerical calculations with a few number of modes.

a) The Turbulent Model

Now we propose a qualitative explanation of the numerical results in the frame of the strong turbulent model. Here it is more suitable to use instead of eq. (10) - (11) the equations in physical normalisations, namely:

$$\rho_s^2\left(\frac{\partial}{\partial t}+D_B\overline{V}_\perp\cdot\nabla-\mu_\perp\Delta_\perp\right)D_\perp\varphi-V_g\frac{\partial n}{\partial y}=-D_\parallel\nabla_\parallel^2(\varphi-n),$$

$$\left(\frac{\partial}{\partial t}+D_B\overline{V}_\perp\cdot\nabla-D_\perp\Delta_\perp\right)n\;=\;-D_\parallel\nabla_\parallel^2(\varphi-n), \tag{22}$$

where $D_B=\frac{cT_e}{eB_o}, V_g=C_s\rho_s/R,\ D_\parallel=V_{Te}^2/\nu_{ei},\ \varphi=e\phi/T_e,\ n\;=\;n/n_o,$

$$\vec{V}_\perp=[\vec{e}_z\nabla\varphi].$$

The solution of (22) determines the structure of vorticity and particle fluxes: $\langle V_x\Omega\rangle$, $\Omega\;=\;\Delta_\perp\varphi$ and $\langle V_x n\rangle$. The obtained qualitative understanding of the properties of $\langle P_x\rangle$ and $\langle\Gamma_x\rangle$ can be obtained from quasilinear theory. For the averaged variables we get from (22):

$$\frac{\partial}{\partial t}\langle\Omega\rangle\;+\;\frac{\partial}{\partial x}\langle P_x\rangle=0,$$

$$\frac{\partial}{\partial t}\langle n\rangle\;+\;\frac{\partial}{\partial x}\langle\Gamma_x\rangle=0, \tag{23}$$

where $\langle\Omega\rangle\;=\;\langle\Delta_\perp\varphi\rangle$,

$$\langle P_x\rangle=D_B\langle V_x\Delta_\perp\varphi\rangle-\mu_\perp\frac{\partial}{\partial x}\langle\Delta_\perp\varphi\rangle,$$

$$\langle\Gamma_x\rangle=D_B\langle V_x n\rangle-D_\perp\frac{\partial}{\partial x}\langle n\rangle. \tag{24}$$

From the linearized system we can express the perturbations of $\tilde{\varphi}$ and $\tilde{n}$ through terms proportional to $\frac{\partial\langle\Omega\rangle}{\partial x}$ and $\frac{\partial\langle n\rangle}{\partial x}$.

$$\begin{pmatrix} \tilde{\omega} + i\nu_\Omega - \dfrac{k_y V_g + ik_\parallel^2 D_\parallel}{K_\perp^2 \rho_s^2} & \\ -ik_\parallel^2 D_\parallel & \tilde{\omega} + i\nu_n \end{pmatrix} \begin{vmatrix} \tilde{\varphi} \\ \tilde{n} \end{vmatrix} = k_y D_B \tilde{\varphi} \cdot \begin{vmatrix} \dfrac{1}{k_\perp^2} & \dfrac{\partial \langle \Omega \rangle}{\partial x} \\ \dfrac{\partial \langle n \rangle}{\partial x} & \end{vmatrix} \tag{25}$$

Inserting the solution of (25) into (24), one can get the following expressions for the fluxes in the Fourier representation:

$$\begin{aligned} \langle P_x \rangle &= \mathrm{Re}\left[D_B \sum_k i k_y \frac{\Delta\Omega}{\Delta} \left\langle \varphi_k \varphi_k^+ \right\rangle \left(-k_\perp^2 \right) \right] - \mu_\perp \frac{\partial}{\partial x} \langle \Omega \rangle, \\ \langle \Gamma_x \rangle &= \mathrm{Re}\left[D_B \sum_k i k_y \frac{\Delta n}{\Delta} \left\langle \varphi_k \varphi_k^+ \right\rangle \right] - D_\perp \frac{\partial}{\partial x} \langle n \rangle, \end{aligned} \tag{26}$$

where

$$\Delta = \begin{vmatrix} \tilde{\omega} + i\nu_\Omega - \dfrac{k_y V_g + ik_\parallel^2 \; D_\parallel}{k_\perp^2 \rho_s^2} & \\ -k_\parallel^2 \; D_\parallel & \tilde{\omega} + i\nu_n \end{vmatrix}; \quad \Delta\Omega = k_y D_B \begin{vmatrix} \dfrac{1}{k_\perp^2} \dfrac{\partial \langle \Omega \rangle}{\partial x} - \dfrac{k_y V_g + ik_\parallel^2 D_\parallel}{k_\perp^2 \rho_s^2} & \\ \dfrac{\partial \langle n \rangle}{\partial x} & \tilde{\omega} + i\nu_n \end{vmatrix}$$

$$\Delta n = k_y D_B \begin{vmatrix} \tilde{\omega} + i\nu_\Omega & \dfrac{1}{k_\perp^2} \dfrac{\partial \langle \Omega \rangle}{\partial x} \\ -k_\parallel^2 \; D_\parallel & \dfrac{\partial \langle n \rangle}{\partial x} \end{vmatrix}$$

$$\tilde{\omega} = \omega - k_y V_o(x), \; V_o(x) = \frac{\partial \langle \varphi \rangle}{\partial x}, \; \nu_\Omega = \mu_\perp k_\perp^2 + \frac{k_\parallel^2 \; D_\parallel}{k_\perp^2 \rho_s^2}, \; \nu_n = k_\perp^2 D_\perp + k_\parallel^2 D_\parallel.$$

To simplify this model we consider the fluid limit $D_\parallel \to 0$:

$$\langle P_x \rangle = -(\mu_\perp + \mu_{\perp tr}) \frac{\partial \langle \Omega \rangle}{\partial x} + b \frac{\partial \langle n \rangle}{\partial x}, \tag{27}$$

$$\langle \Gamma_x \rangle = -(D_\perp + D_{\perp tr}) \frac{\partial \langle n \rangle}{\partial x},$$

where

$$\mu_{\perp tr} = D_B^2 \sum_{k\omega} \frac{k_y^2 \nu_\Omega}{\tilde{\omega}^2 + \nu_\Omega^2} \left\langle \varphi_k \varphi_k^+ \right\rangle, \quad D_{\perp tr} = D_B^2 \sum_{k\omega} \frac{k_y^2 \nu_n}{\tilde{\omega}^2 + \nu_n^2} \left\langle \varphi_k \varphi_k^+ \right\rangle$$

$$b = -D_B^2 \sum_{k\omega} \frac{k_y^4 (\nu_\Omega + \nu_n) V_g V_o(x)}{\left(\tilde{\omega}^2 + \nu_\Omega^2\right)\left(\tilde{\omega}^2 + \nu_n^2\right)} \left\langle \varphi_k \varphi_k^+ \right\rangle.$$

We remind that $\left\langle \varphi_k \ \varphi_k^+ \right\rangle$ is dimensionless. Note, that the cross gradient term is zero in the density flux, but in the vorticity flux the cross term vanishes (b = 0) only in the case of shearless flow, V = const, because of the symmetry of the spectrum $\left\langle \varphi_k \ \varphi_k^+ \right\rangle$ in the frame moving wiht the velocity V. Obviously, for the large scale modes the transition into the moving frame is impossible in the case of shear flow $V_o(x) \approx V'_o x$. Because the large scale modes play the main role in the energy transfer dynamics (being the most unstable only they gain energy from the nonequilibrium density distribution), the more adequate description is to consider the amplitude of the most unstable mode as the control parameter. Due to nonlinear mixing processes there are two ways of energy dissipation: by means of a cascade towards the stable small scale modes and by means of shear flow generation. Thus, two parameters arise: the averaged spectral intensity $I = \sum_{k\omega} \left\langle \varphi_k \ \varphi_k^+ \right\rangle$ and the characteristic velocity of the shear flow U. To provide an energy source for the instability, the average density gradient N = <n> must be incorporated in the model. The following set of model equations can be obtained:

$$\frac{\partial U}{\partial t} = -\left(\frac{1}{\tau_{0U}} + \frac{I}{\tau_{1U}}\right) U + \beta U I N, \tag{28}$$

$$\frac{\partial N}{\partial t} = -\frac{N}{\tau_{0N}} + \frac{I}{\tau_{1N}} (N - N_0), \tag{29}$$

$$\frac{\partial I}{\partial t} = -\left(\gamma_o \left(1 - U^2\right) - \frac{1}{\tau_1} - D I\right) I. \tag{30}$$

Rough estimates have been used here, for example $\frac{\partial}{\partial x}(\mu_\perp + \mu_{\perp tr})\frac{\partial\langle\Omega\rangle}{\partial x} \to \left(\frac{1}{\tau_{0U}} + \frac{I}{\tau_{1U}}\right) U$, because $\langle\Omega\rangle = d^2U/dx^2 \to U/a^2$. This term represents the viscous damping of the shear flow due to ordinary and turbulent viscosity. The last term in the velocity equation is responsible for the flow generation. In the spectrum equation the first term describes both the linear instability and the stabilising effect due to the shear flow, the second term yields small linear damping and the last one corresponds to the nonlinear stabilisation. The same type of equations was proposed recently by other authors [15], [16].

The proposed model demonstrates a variety of phenomena (regime with saturation, periodic oscillations, doubling of period, etc.), which is in surprisingly good agreement with the behaviour of the full set of equations. So we dare say, we have got an insight into the phenomenon of shear flow generation on the plasma periphery.

If we take an interest in only the L-H transitions itself, without any ELM activity, then we can consider the case of N = 1 and use two equations for V and I. This system coincides with the recently proposed model for the L-H transition from the paper [16]. The main deficiency of this model is that we do not know the exact expressions for the coefficients in (22) - (24).

b) The Model With a Small Number of Harmonics (SM-model).

It follows from the numerical calculations for small viscosity $\mu_\perp$ and diffusivity $D_\perp$ ($\mu_\perp \sim D_\perp \sim 0.01$ - 0.1) that there are a few dominant harmonics in the system, typically 5 - 8. This allows us to construct the model with a small number of harmonics (SM-model) taking into account only the amplitudes of the most important harmonics. This approach with a reasonable choice for the harmonics gives us the qualitatively correct description of the process. For example, the well-known Lorentz model, describing the thermal convection in the gravity force field, takes into account three parameters: the amplitude of the vortex, X, of the mode $\phi = X*\cos(k_y*y)*\sin(k_x*x)$, the perturbation of the density of the vortex, Y, of the mode $\tilde{n} = Y*\sin(k_y*y)*\cos(k_x*x)$ and the distortion of the average radial density profile, Z, of the mode $\tilde{n} = Z*\sin(2*k_x*x)$. The Lorentz model does not take into account the possibility of the sheared flow generation. Adding more harmonics can account for this effect. First of all, we should take into account the amplitude of the sheared flow $\phi \sim V*\sin(k_x*x)$, but this is not yet sufficient as the

square nonlinearity in the initial equations does not allow to interact with other harmonics in the Lorentz model. Therefore, we should also take into account the distortion of the vortex and the correction in the density perturbation.

In principal two functions, ϕ and n, can be described for our system of equations using 2*6 = 12 amplitudes of the appropriate modes. Let us show that for every fixed y the quantities ϕ and n can be represented as a sum of the even, ϕ_+, and the odd, ϕ_-, modes. For every poloidal cross section there are particular functions ϕ_+ and ϕ_-, but for this small-number approach it is sufficient to chose the same functions $\phi_+ \sim \sin(k_x*x)$ and $\phi_- \sim \sin(2*k_x*x)$; we remind that the calculation is performed in the square box $0<x<1$, $0<y<1$ and that $\phi(0, y) = \phi(1, y) = 0$). We can repeat this argument for the amplitude $\varphi_+(y)$ and $\varphi_-(y)$ as functions of y. For a small number of modes this can be chosen approximately as a sum of the three terms: the even part consists of the average part, which does not depend on y, the term proportional to $\cos(k_y*y)$ and the odd part proportional to $\sin(k_y*y)$. Then, for example, the potential ϕ can be written as:

$$\begin{aligned}\phi = &\left[\phi_{10} + \phi_{1s}*\sin(k_y*y) + \phi_{1c}*\cos(k_y*y)\right]*\sin(k_x*x) + \\ &\left[\phi_{20} + \phi_{2s}*\sin(k_y*y) + \phi_{2c}*\cos(k_y*y)\right]*\sin(2*k_x*x),\end{aligned} \tag{31}$$

where the six amplitudes $\phi_{m\alpha}$ are functions of time only. In the same fashion another six amplitudes appear in the representation of n, $n_{m\alpha}$. All these 12 amplitudes are connected by the nonlinearity. In conclusion, there are 12 coupled equations but the subsequent analysis shows that only a few of them are important.

We chose the minimal model, namely a five-mode model, where only ϕ_{10}, ϕ_{1c}, ϕ_{2s} and n_{20} n_{1s}, are taken into account:

$$\begin{aligned}\phi &= \left[V + X*\cos(k_y*y)\right]*\sin(k_x*x) + W*\sin(k_y*y)*\sin(2*k_x*x), \\ n &= Y*\sin(k_y*y)*\sin(k_x*x) + Z*\sin(2*k_x*x).\end{aligned} \tag{32}$$

Here X, Y, Z, V, W denote the amplitudes of the harmonics. Inserting expressions (32) into eqs. (6)-(7) and equating terms for equal harmonics, we can get the

following system of ordinary differential equations, where the terms inside the box form the Lorentz system:.

$$\frac{dX}{d\tau} = -\left(\frac{\sigma_1}{k_\perp{}^2} + \mu_\perp k_\perp^2\right)\cdot X + \gamma_g \cdot Y - V\cdot W, \tag{33}$$

$$\frac{dY}{d\tau} = -\left(\frac{1}{\tau_\parallel} + D_\perp k_\perp^2\right)\cdot Y + \gamma_g\ X + X\cdot Z, \tag{34}$$

$$\frac{dZ}{d\tau} = -4k_x^2\cdot D_\perp \cdot Z - X\cdot Y, \tag{35}$$

$$\frac{dV}{d\tau} = -\mu_\perp k_x^2\cdot V + X\cdot W, \tag{36}$$

$$\frac{dW}{d\tau} = -\left[\frac{\sigma_1}{4k_x^2+k_y^2} + \mu_\perp\left(4k_x^2+k_y^2\right)\right]\cdot W + \frac{3}{4}\frac{k_y^2}{\left(4k_x^2+k_y^2\right)}\cdot X\cdot V, \tag{37}$$

here $k_\perp^2 = k_x^2 + k_y^2$ and new variables are introduced
$X \to \alpha_x X,\ Y \to \alpha_y Y,\ Z \to \alpha_z Z,\ V \to \alpha_v V,\ W \to \alpha_w W,$

where $\alpha_x = \frac{\sqrt{2}}{k_x k_y},\ \alpha_y = \frac{k_\perp \sqrt{g_B}\sqrt{2}}{k_x k_y \sqrt{g_n}},\ \alpha_z = \frac{k_\perp}{k_x k_y}\sqrt{\frac{g_B}{g_n}},\ \alpha_v = \frac{k_\perp}{k_x k_y\sqrt{3k_x^2+k_y^2}},$

$\alpha_w = \frac{2}{3}\frac{\sqrt{2}k_\perp}{k_x k_y\sqrt{3k_x^2+k_y^2}},\ \gamma_g{}^2 = \frac{g_B g_n k_y^2}{k_\perp^2}.$

System (33) - (37) describes the generation of sheared flow. This can be seen from the equilibrium solution of the system. For the stationary state we have the following non-trivial solution:

$$X_0^2 = \frac{4}{3}\cdot\mu_\perp\frac{k_x^2}{k_y^2}\left[\sigma_1 + \mu_\perp\cdot\left(4k_x^2+k_y^2\right)^2\right],$$

$$Y_0 = \gamma_g\cdot X_0 \Big/ \left[\frac{1}{\tau_\parallel} + D_\perp k_\perp^2 + \frac{X_0^2}{4k_x^2 D_\perp}\right],$$

$$Z_0 = -X_o Y_0 / \left(4k_x^2 D_\perp\right),$$

$$W_0 = \mu_\perp \cdot k_x^2 \cdot V_0 / X_0,$$

$$V_0^2 = \frac{4}{3} \frac{\left[\sigma_1 + \mu_\perp\left(4k_x^2 + k_y^2\right)\right]}{k_y^2} \left\{ \frac{\gamma_g^2}{\left[\frac{X_0^2}{4k_x^2 D_\perp} + \frac{I}{\tau_\parallel} + D_\perp\left(k_x^2 + k_y^2\right)\right]} \right.$$

$$\left. - \left[\frac{\sigma_1}{k_x^2 + k_y^2} + \mu_\perp \cdot \left(k_x^2 + k_y^2\right)\right] \right\}. \qquad (38)$$

It is not difficult to see from (38) that there exists a critical value for γ:

$$\gamma_{g1}^2 = \left[\frac{X_0^2}{4k_x^2 D_\perp} + \frac{I}{\tau_\parallel} + D_\perp\left(k_x^2 + k_y^2\right)\right] \cdot \left[\frac{\sigma_1}{k_x^2 + k_y^2} + \mu_\perp \cdot \left(k_x^2 + k_y^2\right)\right] \qquad (39)$$

For $\gamma_g < \gamma_{g1}$ only equilibria with V = 0 exists. But for $\gamma_g > \gamma_{g1}$ there exist equilibria with non-zero V, i.e. the generation of flow takes place. If this threshold γ_{g1} is exceeded by a small amount, the corresponding equilibria are stable and solutions of the system (33) - (37) approach asymptotically one of these. Due to the possibility of a different sign for X_0 and V_0 there are four formal equilibrium solutions. On Fig. (6a) typical solutions for this regime are plotted, where

$$q_x = D_\perp \left(1 + \frac{\sqrt{1 + \left(k_y / \pi\right)^2}}{k_y} Z\right) \qquad (40)$$

is the particle flux on the boundary for the small-parametric model.

Numerical calculations yield that there is another critical value of γ_g: $\gamma_g > \gamma_{g2}$, for which the previous equilibria become unstable. The typical behaviour for this regime is shown on Fig. 6b. For $\gamma_g = \gamma_{g2}$ the system bifurcates into an ELM regime. The evolution of X and V now look like the Volttera model.

It is interesting to compare the solutions of the system (33) - (37) with the results of the numerical simulation. On Fig. 7 the dependence of the average flux $Q = \lim_{\tau\to\infty} \frac{1}{\tau} * \int_0^\tau q_x(t)\,dt$ is shown against γ_g. There are two distinctive features of Q: Firstly the saturation of the flux with increasing γ_g and, secondly, the fast drop in Q when γ_g approaches γ_{g2}. The first fact is easily explained by making use of the solutions (38). For this equilibrium we have $Z_0 / \gamma_g \approx 1$ if $X_0^2 > 4k_x^2 k_y^2 D_\perp^2$ (this is usually satisfied, then Q ≈ 3, as it follows from (40), and it agrees well with the numerical simulation). For larger values of γ_g, when the equilibria become unstable and do not exist anymore, this analysis still makes sense. In this case the system moves along limiting cycles in phase space 'around' unstable equilibria and after averaging over time the average value of Z settles to a value close to, but a little less than, Z_0. The second phenomenon of our model, namely the drop of q_x for $\gamma_g = \gamma_{g2}$ (see Fig. 7), also qualitatively agrees with the behaviour of the full system. The value of this drop depends on σ_1 and the maximum equals 20% (for $\sigma_1 = 5$) for the five-modes model.

Thus, the proposed small-parametric model reproduces many features of the behaviour of a plasma near the separatrix: the generation of shear flow, the appearance of ELMs, and the improvement of confinement (decrease of the particle flux) with increasing γ_g (temperature), i.e. the L-H transition. The model, however, does not give a definite direction for the rotation of the plasma. There are solutions with a positive and with a negative sign of V, as the equations do not change under a transformation $V \to -V$, $W \to -W$ where the other amplitudes do not change sign. The initial equations (10) - (11) have just the same specific symmetry which does not allow to determine the direction of the flow. From experiments it is known that the real sign of the velocity corresponds to preferential losses of electrons; therefore the plasma is charged positively.

For the explanation of the sign of the velocity we should take into account additional effects which destroy the symmetry of the system (33) - (37). The simplest effect is the appearance of a small initial (seed) field due to preferential losses of particles of definite sign. This effect can be taken into account by introducing some source V_*, i.e. an initial electrical field, in equation (36) for V:

$$\frac{dV}{d\tau} = -\mu_\perp \cdot k_x^2 * (V - V_*) + X * W. \qquad (41)$$

This term breaks the symmetry of the system. Naturally, it is not of interest to introduce a term of order unity into this equation. But we can show that for a

definite determination of the sign of the velocity it is sufficient to introduce a V_* in the order of the initial perturbation, i.e. when V_* is more than two orders of magnitude less than the final velocity.

The interpretation of this effect is as follows: For $V_* = 0$ there are two equilibrium solutions with opposite flow $V = \left(\begin{smallmatrix}+\\-\end{smallmatrix}\right) V_0$. On the other hand, two limiting circles occur to which the solutions should go. The boundary between these two regions scales symmetrically (this is a property of the system (31) - (37)) around the origin of the coordinates, i.e. through the point $X = Y = Z = V = W = 0$. If the initial conditions spread homogeneously inside a small 'sphere' around the zero point then the probability for a trajectory near each cycle is the same. If $V_* \neq 0$ then three equilibria appear since now we have a cubic equation for V_0, and the third root is far away from zero. But, more importantly, the boundary between these cycles moves from zero to some small distance R_*, being proportional to V_*. Now the boundary divides the 'sphere' of initial conditions into two, non-equal parts. Therefore, the near-definite, limiting cycle becomes not probable. If V_* is equal or larger than the amplitude of the initial perturbation then a definite sign of the velocity becomes inevitable. This implies that values of V_* in the order of the amplitude of the initial perturbations control the sign of the shear velocity. In Fig. 8 (in the (X–R) plane, where $R^2 = X^2 + Y^2 + Z^2 + V^2 + W^2$) the initial points of the trajectories, which are going to the limit cycle with $V*V_* < 0$, are displayed. There exists a minimal R_{min}, depending on V_*, such that for $R > R_{min}$ the trajectory finds a definite cycle (or the system generates a definite sign of velocity). In Fig. 9 the dependence of this R_{min} on V_* is displayed. Clearly R_{min} is proportional to V_0 which confirm our previous conjecture.

6. DISCUSSION

Experimental observations, together with the following considerations, support the model based on resistive interchange perturbations at the plasma edge:

1. The thermal energy of the plasma $W_{th} = n*T$ is often comparable or larger than the magnetic energy due to the current $W_J = B_\perp^2 / 8*\pi$; $\beta_J \sim 1$. Therefore it is difficult to understand why magnetic activities are easily observed (kink, tearing, sawtooth instabilities) but why instabilities connected with the pressure are not detected;

2. There are very long $(L_\parallel \sim 10m)$ and narrow (d ~ 0.01m) filaments at the edge (ASDEX [3], TFTR [2]);

3. Fluctuations at the boundary are anti-drift: $e^*\phi / T_e >> n / n_0$ [17], this is a typical relation for flute-type perturbations;

4. With increasing temperature ELMs at first appear and then disappear. This fact supports the concept of resistive instabilities;

5. Outside the separatrix the fluctuations propagate in the ion diamagnetic drift direction, which is very natural for flute-type perturbations. However, drift-type fluctuations propagate usually in the electron drift direction.

   From our model we can estimate the coefficient of the turbulent diffusion D_{RI} and the thickness of the SOL, if its extend is indeed determined by the resistive interchange.

   Using dimensional estimates for the coefficient of the turbulent diffusion (or thermal conductivity) D_{RI} we can write $D_{RI} = \gamma_0 / k_0^2$.

   For our case:

$$D_{RI} = \left(\omega_g / k_\parallel C_A\right)^2 * D_M . \qquad (42)$$

From this expression it follows that $D_{RI} < D_M$, as for the ideally flute-stable plasma $\left(\omega_g / k_\parallel C_A\right)^2 < 1$. The expression (42) can be rewritten in the following form:

$$D_{RI} = \left(L_\parallel^2 / x_0 R\right) * \nu_{ei} * \rho_e^2, \tag{43}$$

where $k_\parallel = 1/L_\parallel$, ρ_e is the electron Larmor radius, ν_{ei} the electron-ion collision frequency and $x_0 = \left(1/P_0 * dP_0/dx\right)^{-1}$.

The expression (43) is correct for the volume conductivity. For the influence of the end plate we should change ν_{ei} to $\nu_{ef} = \left(v_{Te}/L_\parallel\right) * (M/m)^{1/2}$. In this case Eq. (43) can be brought into a form very close to the gyro-Bohm value [14]:

$$D_{RI} = \left(L_\parallel / R\right) * C_s * \rho_{is}^2 / x_0, \tag{44}$$

where $C_s = (T_e/M)^{1/2}$ is the sound velocity, $\rho_{is} = C_s / \omega_{Bi}$.

In order to obtain an estimate on the width of the SOL, x_0, related to the resistive interchange instabilities one should use the continuity equation:

$$D_{RI} * \frac{d^2 n_0}{dx_0^2} = \frac{n_0}{\tau_\parallel}, \tag{45}$$

supposing that longitudinal losses scale with the sound velocity $\tau_\parallel = L_\parallel / C_s$ where $D_{RI} = \gamma_0 / k_0^2$. From (45) we then can get the following approximation for x_0: $\left(k_0 * x_0\right)^2 = \gamma_0 * \tau_\parallel$. Using the expressions for γ_0 and k_0 the dependence of x_0 and D_{RI} on the plasma parameters is established.

For the volume conductivity we obtain

$$x_0^v = 0.24 * \left(T_{i10} + T_{e10}\right)^{1/3} * L_{\parallel m} * n_{013}^{1/3} * T_{e10}^{-2/3} * R_m^{-1/3} * B_{0T}^{-2/3} \text{cm}, \tag{46}$$

here $T_{10} = T_{ev}/10$, $n_{013} = n_0\ (\text{cm}^{-3})\ /10^{13}\ \text{cm}^{-3}$, $B_{0T} = B_0/10^4$.

Inserting the expressions for x_0 into D_{RI} we get

$$D_{RI}^{v} = 1.85*(T_{i10}+T_{e10})^{2/3}*L_{\|m}*n_{013}^{2/3}*T_{e10}^{-5/6}*R_m^{-2}*B_{0T}^{-4/3}m^2/s. \quad (47)$$

For the end plate conductivity we arrive at the ASDEX scaling [13] (for the comparison with the original ASDEX scaling we take into account the possible difference between electron and ion temperatures):

$$x_0^e = 1.0*(T_{i10}+T_{e10})^{1/3}*L_{\|m}^{2/3}*R_m^{-1/3}*B_{0T}^{-2/3}cm. \quad (48)$$

$$D_{RI}^{e} = 0.7*(T_{i10}+T_{e10})^{2/3}*T_{e10}^{1/2}*L_{\|m}^{1/3}*R_m^{-2/3}*B_{0T}^{-4/3}m^2/s. \quad (49)$$

The dependence of x_0 and D_{RI} on T_i for $T_e = 0.3*T_i$ and for ASDEX parameters are plotted in Fig. 10. Here R = 1m, B_0 = 3T, Z = 1, n_{013} = 1, we also suppose that $L_\| \sim \pi*q*R$.

The main difference between the two scalings results from the dependence of the volume conductivity on the density and the inverse dependence on the temperature. But for an edge temperature greater than 100eV the effect of the end-plate conductivity exceeds (neglecting impurities) the volume effects.

In [12] it has been found that the thickness of the layer where large gradients appear is inversely proportional to the magnetic field generated by the current. The same scaling follows from both expressions (46) and (47) if we apply the natural relation $L_\| \sim q*R$.

Another experimental evidence for this class of resistive interchange instabilities is given by the plasma rotation in the ion diamagnetic direction [13]. More details are given in the Appendix.

Let us now consider the condition for the appearance of sheared flow and, hence, the condition for the L-H transition in our model. For this purpose it is suitable to use the small harmonic equations (33) -(37). First of all, from these equations the condition for instability follows: $\left(1-\left(k_\perp^2\mu_\perp\right)\right)/\mu_\perp > \sigma_1$, (we suppose that $D_\perp \approx \mu_\perp$)which for small $\mu_\perp$ can be written simply as:

$$\sigma_1*\mu_\perp < 1. \quad (50)$$

This criterion has the form of

$$\beta > \left(x_0 R / L_{\parallel}^2\right) * (\mu_{\perp} / D_M). \tag{51}$$

It can be rewritten in the following way: $D_{RI} > \mu_{\perp}$, i.e. in the small parameter model the factor D_{RI} appears in spite of the absence of fully developed turbulence and in the absence of a turbulent diffusion coefficient of the order of D_{RI}.

From the condition for the appearance of velocity (39) we obtain after some manipulations the following condition for the L-H transition:

$$\sigma_1 * \mu_{\perp} < 0.1, \tag{52}$$

or

$$\beta > 10 * \left(x_0 R / L_{\parallel}^2\right) * (\mu_{\perp} / D_M). \tag{53}$$

This indicates that the difference between the appearance of the instability, (50) and the condition of the L-H transition, (52) is quantitative rather than qualitative. The numerical factor 0.1 in (52) reflects only the properties of our model and should be obtained from experiments.

The condition (53) strongly depends on the unknown coefficient of the viscosity $\mu_{\perp}$. We propose here the form for $\mu_{\perp}$ and hence for the L-H transition which includes properties made in earlier, different models for the L-H transition. We suppose that the effective viscosity $\mu_{\perp}$ is connected with the losses of particles on banana orbits near the separatrix. In that case the expression for $\mu_{\perp}$ can be estimated as:

$$\mu_{\perp}^{loss} = (\varepsilon)^{1/2} \nu_{ii} \rho_{\theta} x_0. \tag{54}$$

Here ν_{ii} is the ion-ion collision frequency and ρ_{θ} the poloidal ion Larmor radius. Suppose also that D_M is defined mainly by the volume collisions i.e. by the usual Spitzer conductivity, we have finally the following condition for the L-H transition:

$$\rho_\theta > c_1 (M/m)^{1/2} x_0^2 / \left(R\varepsilon^{3/2}\right), \qquad (55)$$

where the constant c_1 has a value of 0.1 or less. The tendency of this result is reasonable: Increasing the poloidal Larmor radius on the edge (ρ_θ) and steepening the density and temperature profiles (smaller x_0) makes the transition into the H phase easier. This is equivalent to the statement that the ratio ρ_θ / x_0^2 should be constant.

7. CONCLUSION

Our model explains the basic phenomena seen in tokamak experiments, namely the edge fluctuations and the L-H transition.

1. In this model the ELMs appear naturally with increasing pressure and disappear with increasing temperature. These perturbations of density or temperature have a small diameter but are very long and occur at the periphery of the plasma. The diameter of these perturbations is in the order (or a little less) of one centimetre and its characteristic period is in the order of a few milliseconds.

2. The shear flow is generated spontaneously and quite effectively. In the simplest case the direction of this flow is accidental but the inclusion of a small difference between the fluxes of the electrons and ions gives a specific direction of the flow.

3. The effect of charge losses on the end plates gives us, unexpectedly, a picture similar to the L-H transition. Namely with increasing pressure (or temperature) the flux of particles (or energy) initially increases but is subsequently suppressed by a factor of 2-3.

Nevertheless, the proposed model has also some unclear points.

1. The classical conductivity is a little too high for the quantitative comparison of the theoretical results with the experiments. If we take into account the end plate conductivity [14] the situation becomes better but now we have to deal with the problem that the physics near the end plate is quite complex.

2. It is very difficult to provide a definite estimate on $\mu_\perp$ and $D_\perp$. The question, whether $\mu_\perp$ and $D_\perp$ are selfconsistantly determined by resistive interchanges or whether these are defined by microinstabilities is still unanswered.

   In this context the proposed theory may help to derive $\mu_\perp$ and $D_\perp$ from experiments as the period of the ELMs depends on them.

3. Additional investigations are required to clarify the influence of the core plasma and to understand the role of non-electrostatic perturbations, especially the significance of flutter to establish the connection between inner- and outer-separatrix plasmas.

APPENDIX

If we take into account the ion and electron diamagnetic effects we can get the following generalization of the dispersion relation Eq. (12):

$$\left(\omega + ik_\perp^2\mu_\perp + \omega_*\right) + i\left(1 + k_\perp^2\rho_s^2 - \frac{\omega*}{\omega + ik_\perp^2 D_\perp + ik_\parallel^2 D_\parallel}\right) * \frac{k_\parallel^2\chi_\parallel}{k_\perp^2\rho_s^2} + \frac{\omega_g^2}{\omega + ik_\perp^2 D_\perp + ik_\parallel^2 D_\parallel} = 0$$

where T_i - T_e, $\omega_* = -(ck_yT/eB)*d\ln(n_0(x))/dx$ denotes the drift frequency, $\chi_\parallel = v_{Te}^2 / \nu_{ei}, \omega_g^2 = \left(C_s^2 k_y^2\right)/\left(x_0 R k_\perp^2\right)$. Dispersion curves for the drift instability and for the resistive interchange are plotted on Fig. 11. It is shown that the branch of oscillations, which was unstable and rotated in the electron diamagnetic direction (Fig. 11(a), curve 'e') begins to rotate, for some $k_\perp$, in the ion diamagnetic direction (Fig. 11 (b), curve 'e') under the influence of the curvature. This result can explain the experiment on ASDEX [13].

REFERENCES

[1] Niedermeyer H. et al., Proc. 18th European Conf. on Contr. Fus. and Plasma Phys., v. 1, p. 301, 1991.

[2] Bush C.E. et al., PPPL-2743, 1991.

[3] Zohm H. et al., Nucl. Fus. v. 32, p. 489, 1992.

[4] Kerner W. et al., Bull. Am. Phys. Soc., v. 36, 2R13, p. 3210, 1991.

[5] Doyle et al., Proc. 18th European Conf. on Contr. Fus. and Plasma Phys. v. 1, p. 247, 1991.

[6] Kukharkin N.N. et al., 14th Int. Conf. on Plasma Phys. and Contr. Nucl. Fus. Res., Wurzburg, Germany 1992.

[7] Newman D.E., Terry P.W., Diamond P.H., Phys. Fluids, v. B4, p. 599, 1992.

[8] Drake J.F. et al., Phys. Fluids, v. B4, p. 488, 1992.

[9] Hassam A.B. //Phys. Fluids, v. B4, p. 485, 1992.

[10] Bazdenkov S.V., Pogutse O.P., JETP Letters, v. 57, p. 410, 1993.

[11] Berk H.L. et al., Nuclear Fus. v. 33, p. 263, 1993.

[12] Kikuchi .M. et al.,20th Int. Conf. on Contr. Fus. and Plasma Phys., v.1, p. 179, Lisboa, 1993.

[13] Endler E. et al., 20th Int. Conf. on Contr. Fus. and Plasma Phys., v.2, p.583, Lisboa, 1993.

[14] Kolesnikov V.E., Nedospasov A.V., Sov. Phys. Dokl., v.32, p.478, 1987.

[15] Parail V. et al., 14th Int. Conf. on Plasma Phys. and Contr. Nucl. Fus. Res., Wurzberg, Germany, 1992.

[16] Diamond P. et al., 20th Int. Conf. on Contr. Fus. and Plasma Phys., Lisboa, 1993.

[17[Connor J.W., 20th Int. Conf. on Contr. Fus. and Plasma Phys., Lisboa, 1993.

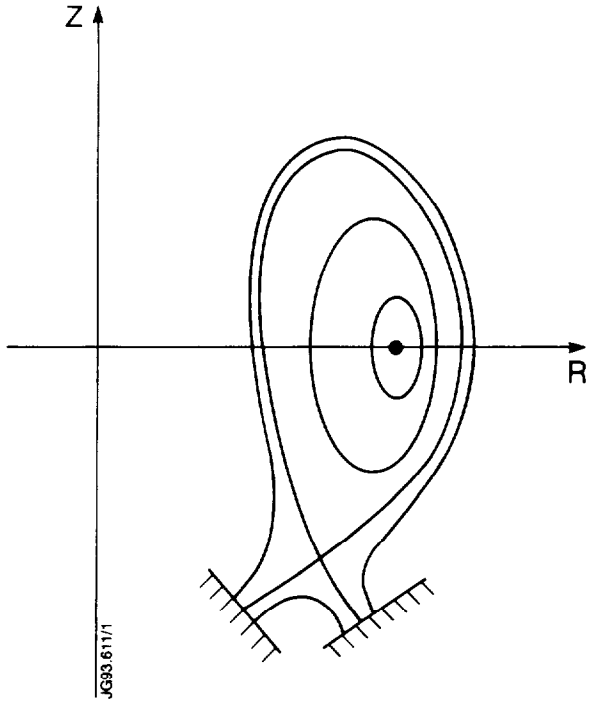

Fig. 1 Typical tokamak divertor geometry.

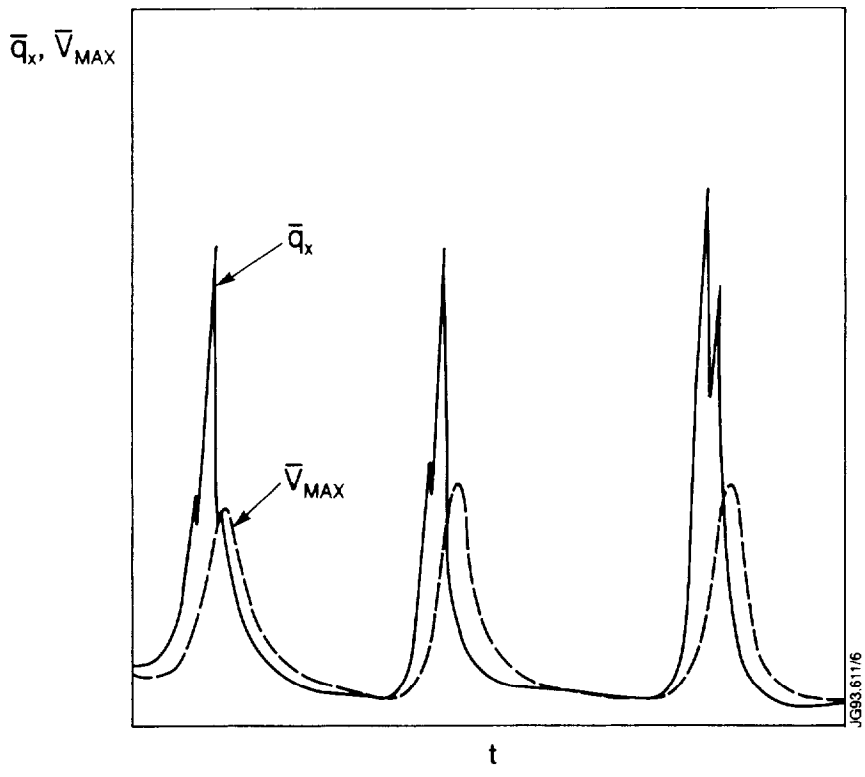

Fig. 2 Temporal evolution of the poloidally averaged particle flux, $\bar{q}_x$, and of the amplitude of the poloidal shear flow, $\bar{V}_{max}$, at the plasma boundary.

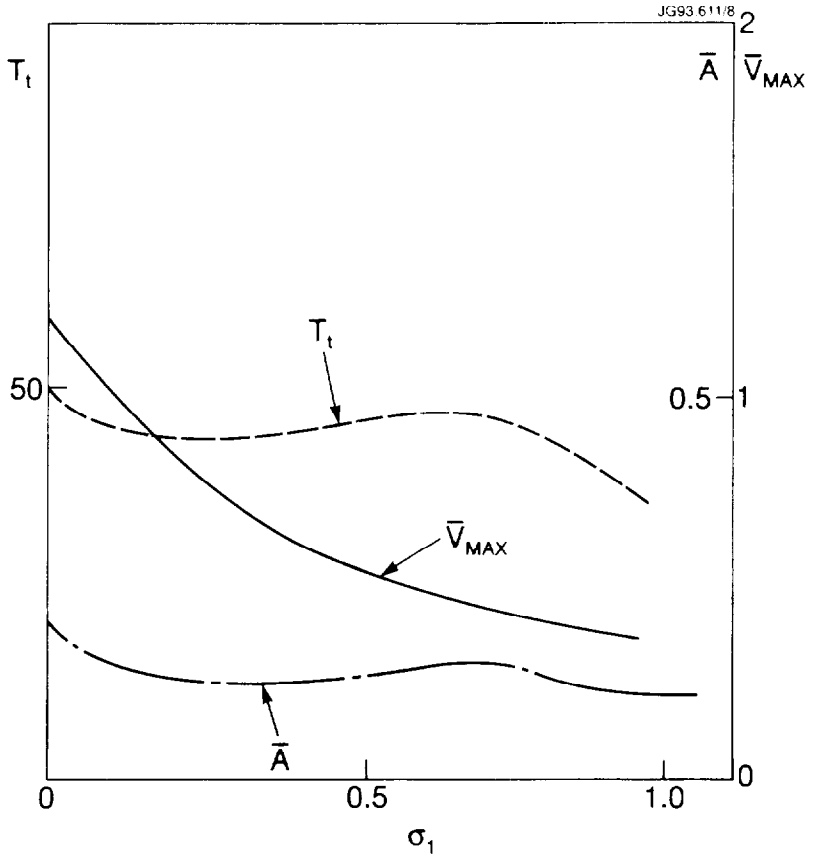

Fig. 3 Dependence of the spike period, T_t, of the spike amplitude, $\bar{A}$, and of the amplitude of the poloidal shear velocity, $\bar{V}_{max}$, on the generalised conductivity $\sigma_1 = (\tau_s / \tau_A) * \beta^{-1/2} * \left(x_0^3 * R_0\right)^{1/2} / L_{\parallel}^2$.

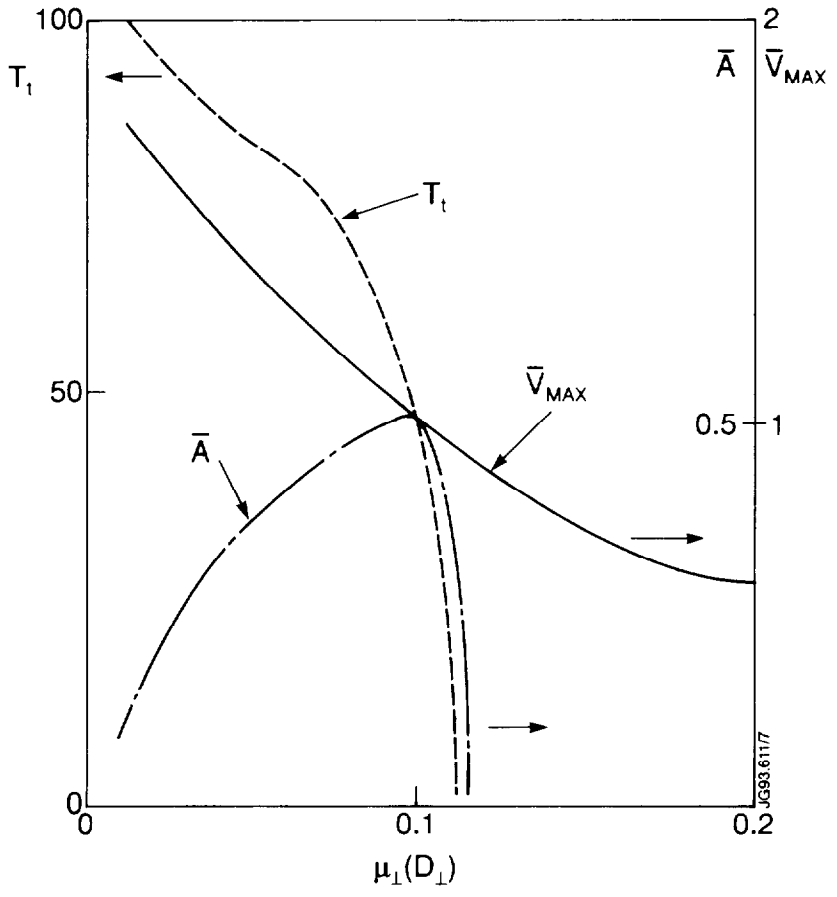

Fig. 4 Dependence of the spike period, T_t, of the spike amplitude, $\bar{A}$, and of the amplitude of the poloidal shear velocity, $\bar{V}_{max}$, on the viscosity $\mu_\perp$ (or $D_\perp$).

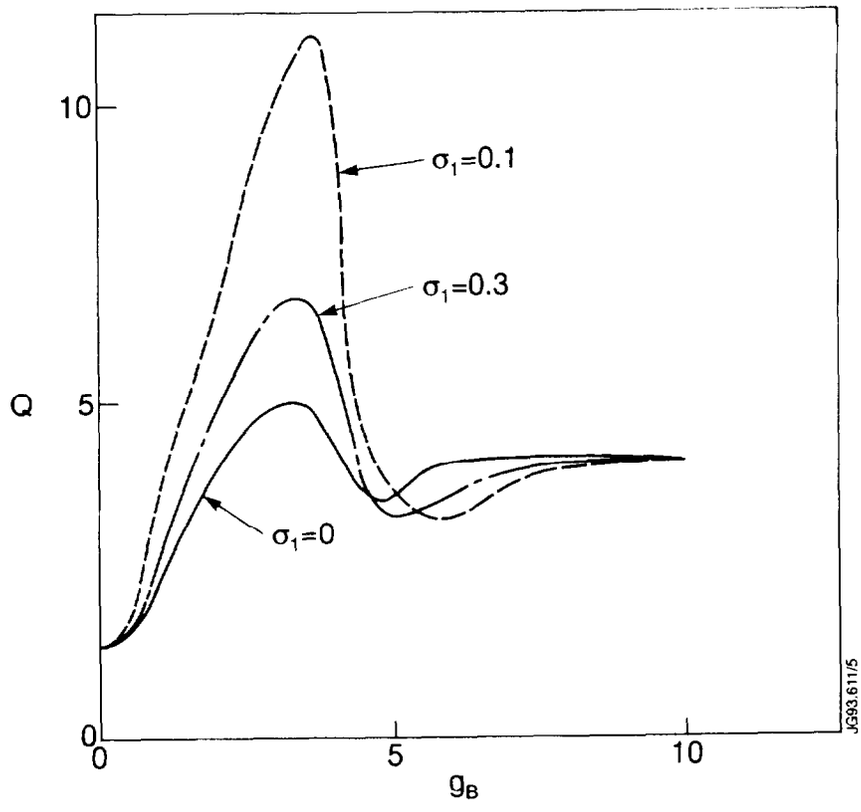

Fig. 5 Dependence of the time averaged particle flux of the boundary, Q, on the parameter g_B (labelling the curvature of the field) for different values of σ_1.

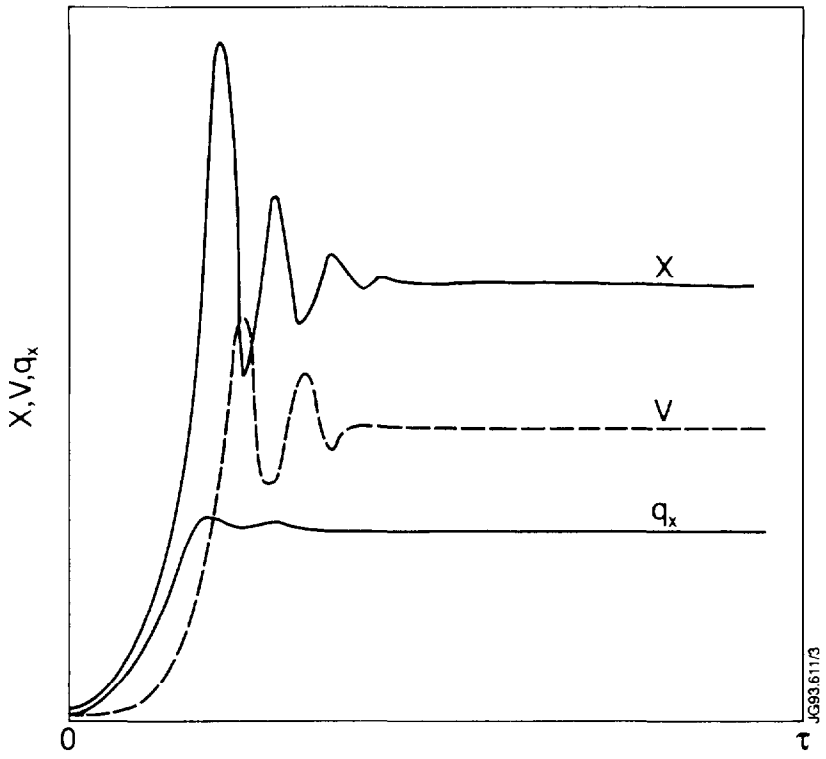

Fig. 6 Typical temporal evolution of the amplitude of the shear velocity, V, of the vortex, X, and of the particle flux at the boundary, q_x, for the case where $\gamma_g < \gamma_{g_2}$ for the SM-model.

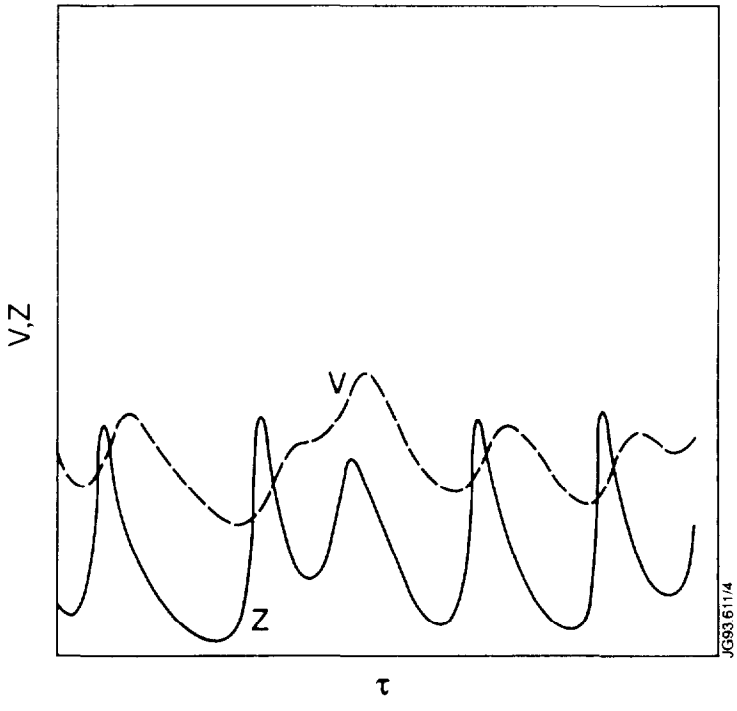

Fig. 6b Typical temporal evolution of the amplitude of the poloidal shear velocity, V, and of the density, Z, for an unstable case where $\gamma_g > \gamma_{g_2}$ for the SM-model.

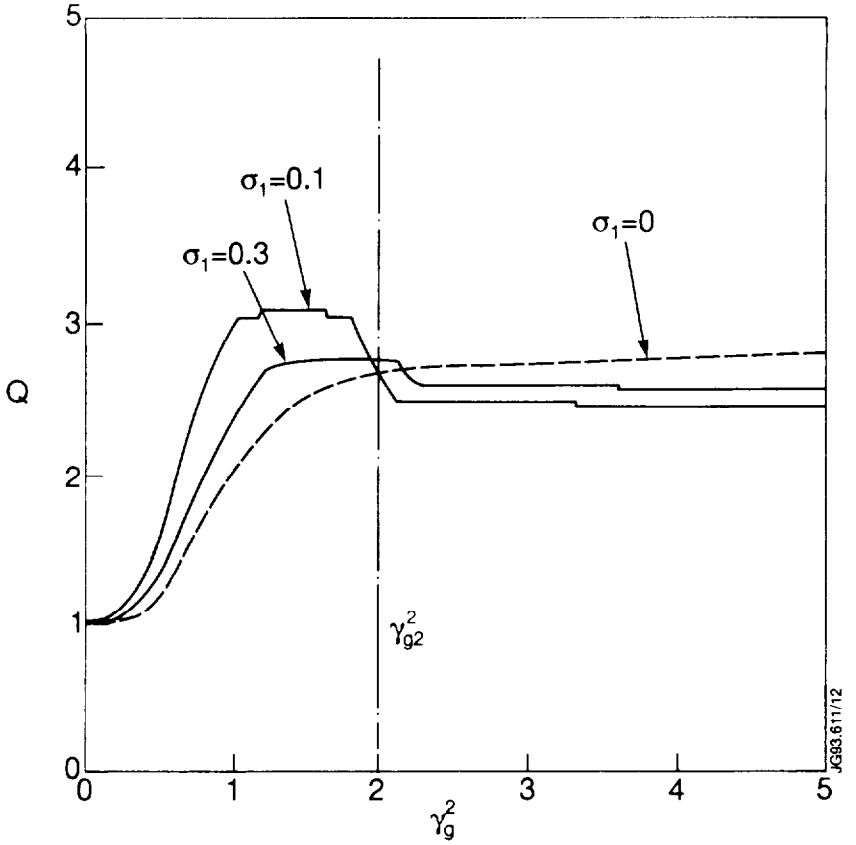

Fig. 7 Dependence of the time averaged particle flux at the boundary, Q, on the growth-rate for three different values of σ_1.for the SM-model.

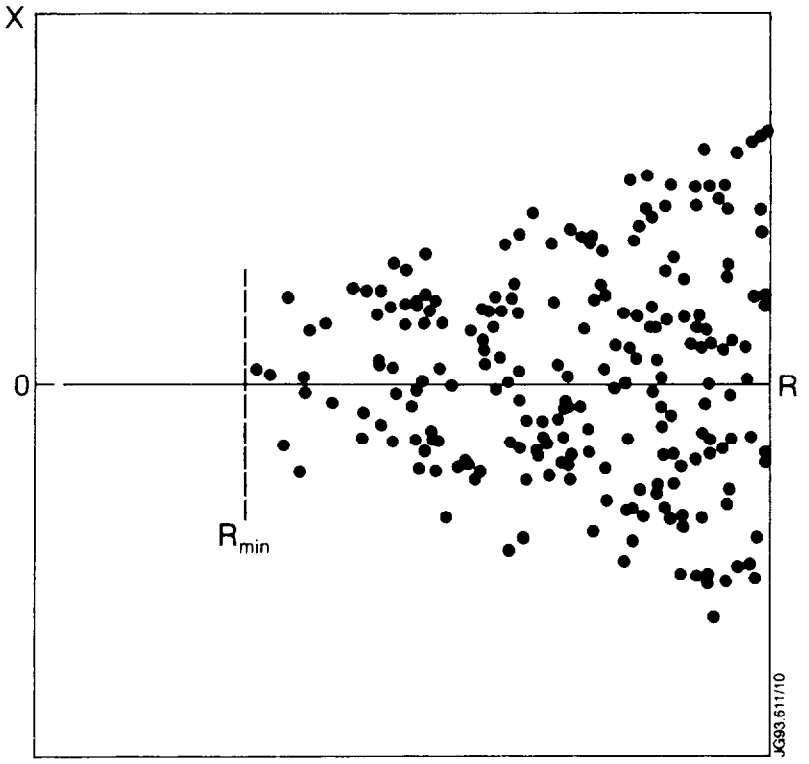

Fig. 8 Initial points of the trajectory in the R-X plane which lead to definite cycles in phase-space.

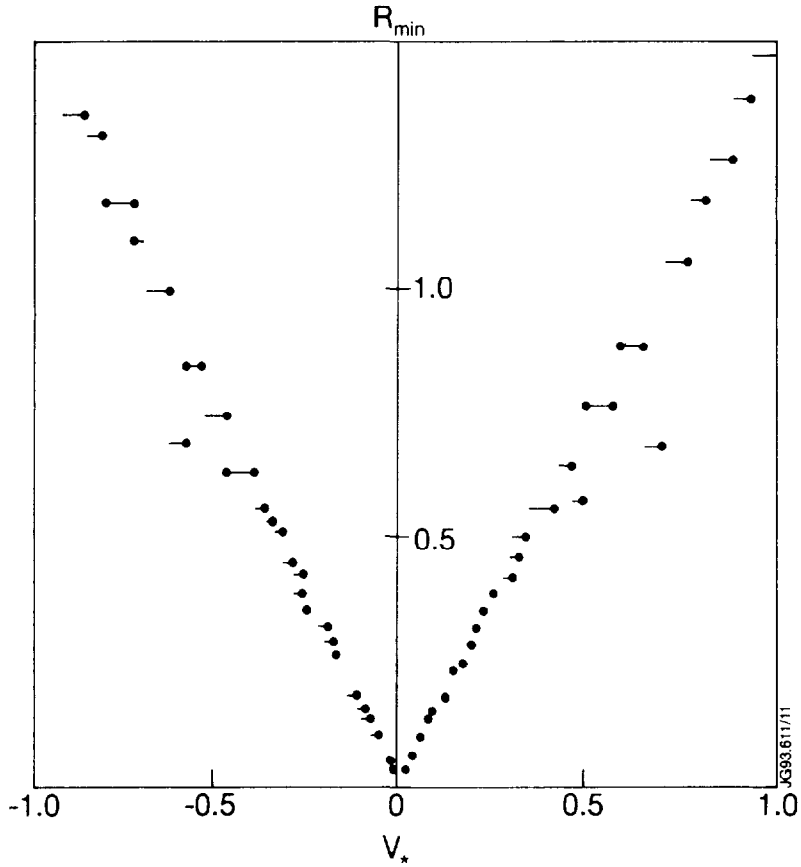

Fig. 9 Radius of the sphere of the initial conditions, R_{min}, which leads to a definite sign of the velocity in dependence of the seed velocity V_*.

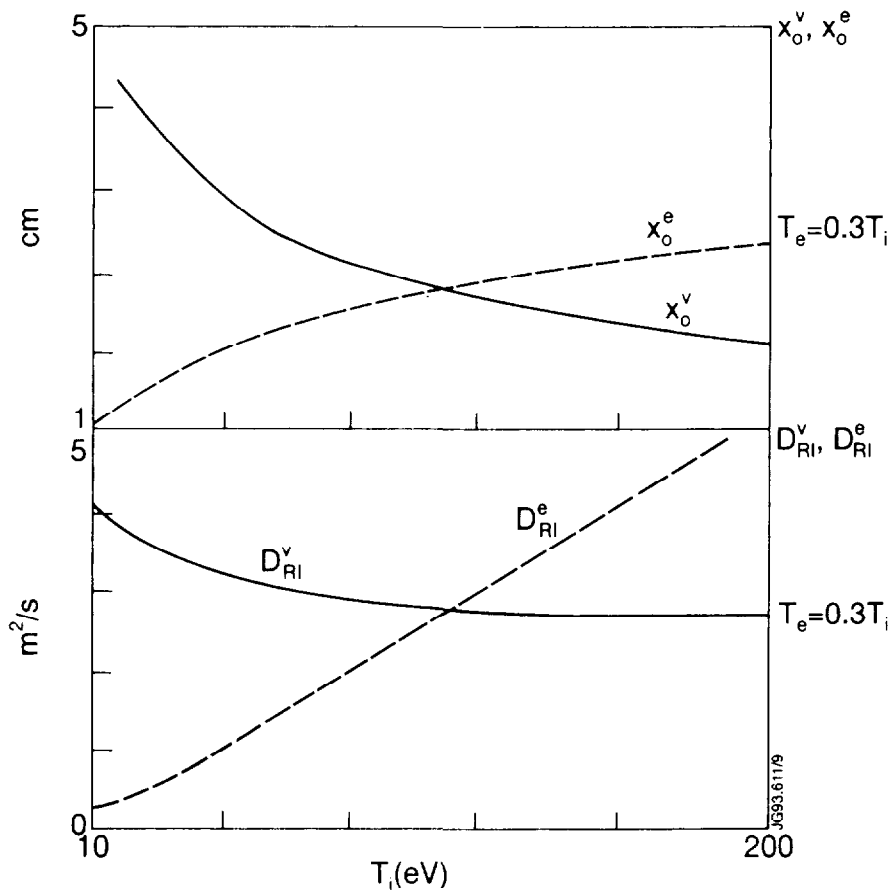

Fig. 10 Dependence of the SOL width and of the diffusion coefficients on the temperature for volume and end-plate conductivity.

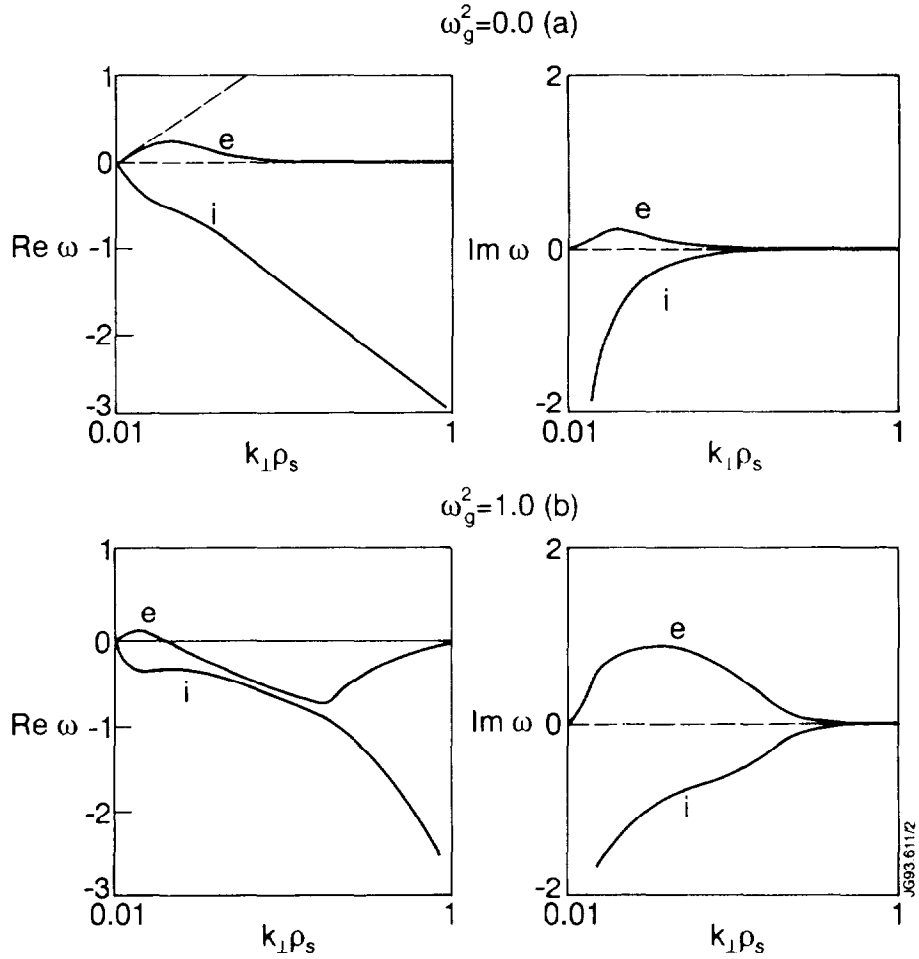

Fig. 11 Real and imaginary parts of the frequency in units of the interchange frequency $\omega_{go}{}^2 = \frac{C_s{}^2}{x_o R_o}\frac{k_y^2}{k_\perp^2}$ in dependence of $k_\perp\rho_s$ for zero curvature, $\omega_g^2 = 0$, and for finite curvature, $\omega_g^2 = 1$. The parameters are chosen as $\frac{k_\parallel{}^2\chi_\parallel\omega_*}{\omega_{go}{}^2} = 0.01$ and $\sqrt{\frac{R_o}{x_o}} = 3$.